Approaches to High Aspect Ratio Triangulations

Mary-Anne K. Posenau

NASA Langley Research Center

Hampton, Virginia

m.a.k.posenau@larc.nasa.gov

Abstract

In aerospace computational fluid dynamics calculations, high aspect ratio, or stretched, triangulations are often used to adequately resolve the features of a viscous flow around bodies. In this paper, we explore alternatives to the Delaunay triangulation which can be used to generate high aspect ratio triangulations of point sets. The method is based on a variation of the lifting map concept which derives Delaunay triangulations from convex hull calculations.

1 Introduction

In computational fluid dynamics (CFD) applications, the problem domain must be discretized into meshes (or grids) over which the governing equations of fluid dynamics are solved. In general, calculations which take the viscosity of fluids into account result in very high solution gradients normal to surfaces, and very small solution gradients tangent to surfaces, with the effect diminishing with distance from the surface. Effective use of the computational effort required to solve the governing flow equations results when a grid contains high aspect ratio, surface-conforming elements near bodies and low aspect ratio elements at a distance. This study investigates more robust alternatives to the primarily heuristic methods currently used to generate high aspect ratio triangulations.

2 Approaches in Use

Heuristic methods have been primarily used to generate high aspect ratio elements in unstructured grids. These approaches either combine structured grid generation methodologies to generate points followed by a triangulation phase to create the grid, or generate the points and create the triangulation in tandem. Delaunay triangulation is very often unsuitable for the first approach; examples of the inadequacies are described in [1, 2]. Alternative triangulations have been used, such as the min-max triangulation, mainly because they appear to generate grids better suited to CFD applications. Locally optimal, rather than globally optimal, methods are used to generate such grids, primarily due to the cost involved. Another purely heuristic approach is the advancing front technique [3, 4]. This technique uses a greedy method to generate points.
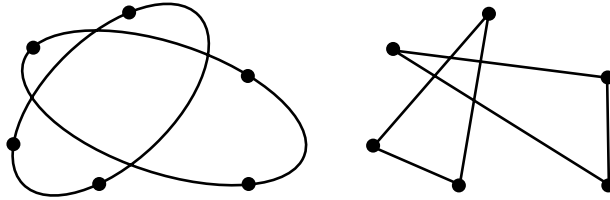
Figure 1: A distance function resulting in an invalid triangulation

A heuristic method to generate stretched triangulations was used by Mavriplis [5]. He recast the n-dimensional planar triangulation problem to an (n+1)-dimensional surface triangulation problem. A control surface was introduced which was related to the aspect ratio, or amount of stretch, desired. Points from the plane were projected to the control surface, and Delaunay triangulation was performed on the surface. Since the method was intimately tied to the point generation method, an assumption of local planarity was valid.

3   A Robust Alternative

A key concept behind the Delaunay triangulation is the empty circumcircle criteria. The method used by Mavriplis essentially modified the concept of distance on the plane used to define the empty circumcircle. By assuming local planarity, circumcircles on the control surface project to circumellipses on the plane. This can be viewed as related to the use of a convex distance function, here an ellipse, to generate a triangulation, similar to the idea of convex distance functions for Voronoi diagrams as described by Chew and Drysdale [6]. The technique used by Mavriplis remains heuristic, however, because of the local planarity assumption. To be truly general, the control surface should be independent of the point generation method, and a general surface triangulation should be employed. A sparse distribution of points projected to a control surface with rapidly changing surface gradients could result in an invalid triangulation; Figure 1 illustrates how a rapidly changing distance function in combination with a sparse set of points could produce overlapping triangles. To generalize the convex distance function formulation to be applicable to the problem at hand, a distance function must vary throughout the plane. Sufficient care must be taken to insure that invalid triangulations could not arise.

To develop an approach which yields high aspect ratio triangulations that is more robust than the ad hoc methods currently in use, we turn to the formulation that relates Delaunay triangulation to convex hulls. A point set lifted onto a paraboloid via orthogonal projection generates a convex hull; when the lower hull is projected back to the plane, this results in a Delaunay triangulation [7]. It is possible to construct other convex bodies in which the convex hull of a point set lifted onto the body similarly produces a triangulation; these triangulations then show a "bias" corresponding to the predominant circumshapes.

First consider the equations of a paraboloid and an arbitrary plane which cuts through the paraboloid. From

$$z = ax + by + c$$
$$z = x^2 + y^2$$

we get the result

$$\left(x - \frac{a}{2}\right)^2 + \left(y - \frac{b}{2}\right)^2 = \frac{a^2 + b^2}{4} + c$$

In other words, by eliminating z we get an expression in x and y which is the equation for a circle, or the projection of the intersection of the plane in 3-space and the paraboloid on the $z = 0$ or 2D plane.

Now, consider a convex object $f(x, y)$. To determine the circumshapes on the plane centered at (x_0, y_0) which correspond to the intersection of a plane $z = ax + by + c$ and the convex object $f(x, y)$, we pose the problem as follows: For any point x_0 and y_0 on the 2D plane, we find the plane in 3-space which is tangent to the convex body at $f(x_0, y_0)$. The intersection of the tangent plane and convex object is simply the point $f(x_0, y_0)$, which projects to the point (x_0, y_0). To "see" the circumshapes centered about this point, the tangent plane must be "pushed" into the convex body by an amount δ to get more than the trivial intersection.

So, the circumshapes about a point (x_0, y_0) are defined by:

$$f(x, y) - (ax + by + c) = 0$$
$$a = \frac{\partial f}{\partial x}\Big|_{x=x_0}$$
$$b = \frac{\partial f}{\partial y}\Big|_{y=y_0}$$
$$c = -ax_0 - by_0 + f(x_0, y_0) + \delta$$

The discussion section describes the results of tests run for different functions $f(x, y)$.

4   An alternative approach

Another way in which the triangulation/convex hull approach might be modified is by changing the projection method used to lift the points to the body. Perspective projection along the line connecting the projection point $(0, 0, z_{proj})$, $(x, y, 0)$, and a convex body is used instead of orthogonal projection. For this section, we use the paraboloid $f(x, y) = x^2 + y^2$, although other convex bodies could be used, as in the previous section. With this method, it is possible under certain conditions for projected points to "miss" the paraboloid entirely, so this scenario is to be avoided by insuring that z_{proj} is sufficiently distant. The circumshapes are defined by:

3

$$\left(x^2 + y^2\right)\left(1 - \frac{c}{z_{proj}}\right)^2 - (ax + by + c)\left(\frac{ax}{z_{proj}} + \frac{by}{z_{proj}} + 1\right) = 0$$

$$a = 2x_0$$
$$b = 2y_0$$
$$c = x_0^2 - y_0^2 + \delta$$

The method used to determine circumshapes on the 2D plane is similar to that used in the previous section; here, the actual values for the partial derivatives are shown since $f(x,y)$ is known in this case. A sketch of the derivation of the circumshape function is given in section A.

An alternative approach is to define a new surface which is based on the perspective projection. Orthogonal projection to this new surface is used so the original (x,y) points are unchanged, but the corresponding z value obtained is what would have resulted from true perspective projection from a point $(0, 0, z_{proj})$ through $(x, y, 0)$ to a paraboloid (in this case, $z_{proj} < 0$). The equation of such a surface follows; a sketch of its derivation is given in section B.

$$z = \frac{1}{4}\left(-\frac{z_{proj}}{\sqrt{x^2 + y^2}} - \sqrt{4z_{proj} + \frac{z_{proj}^2}{x^2 + y^2}}\right)^2$$

5   Discussion of Figures

In this section we discuss several examples of the variation in circumshape for triangulations derived from either convex body alternatives to the paraboloid, or alternative projection. The circumshapes display the various biases of the functions which may be exploited in the triangulations.

Figure 4 shows a set of 200 points randomly selected from a uniform distribution within the box with corners at $(-5, -5)$, $(5, -5)$, $(-5, 5)$, and $(5, 5)$. Each subsequent example uses this test data. It may have been scaled or shifted for different test cases, but any modification to the test set, along with the reason for it, will be indicated during discussion.

The circumshapes derived from both orthogonal and perspective projection examples are shown for regularly spaced (x_0, y_0) for each $f(x, y)$, except as noted in Figure 12. These in general do not correspond to a convex hull, but do illustrate the predominant circumshapes in a particular portion of the 2D plane which result from planes slicing through the convex surface. Since the functions used are continuous, one can infer smoothly changing circumshapes.

The triangulation results in Figures 5-12 are obtained by lifting the test set to the test body $f(x, y)$ using orthogonal projection, finding the lower convex hull with respect to the 2D plane, and projecting these results back to the 2D plane. The triangulation results in Figure 13 are obtained by lifting the test set to a paraboloid using perspective projection, finding the lower convex hull with respect to the projection point $(0, 0, z_{proj})$, and projecting these results back (via perspective projection) to the 2D plane.

Figure 5 illustrates results for a paraboloid, $f(x, y) = x^2 + y^2$. This result corresponds to Delaunay triangulation.

Figure 6 illustrates results for $f(x, y) = x^2 + 10y^2$; circumshapes are plotted for $\delta = 0.05$. A little manipulation of the equations show that the circumshapes about a point (x_0, y_0) are

$$\frac{(x - x_0)^2}{10} + (y - y_0)^2 = \delta$$

which describes ellipses, with centers depending on (x_0, y_0), and identical eccentricity and orientation throughout the plane.

Figure 7 illustrates results for $f(x, y) = x^2 + y^4$; circumshapes are plotted for $\delta = 0.02$. The shapes are constant along one coordinate direction.

Figure 8 illustrates results for $f(x, y) = x^4 + y^4$; circumshapes are plotted for $\delta = 0.02$. Circumcircles predominate along $x = y$ and $x = -y$, with increasing elongation towards the coordinate axes.

Figure 9 illustrates results for $f(x, y) = x^3 + y^3$; circumshapes are plotted for $\delta = 0.09$. The predominant circumshape orientation changes over the plane. Because this body is not convex over the entire plane, the data was translated to the upper right quadrant where the portion of the body to which points are lifted would be convex.

Figure 10 illustrates results for $f(x, y) = x^{1.5} + y^{1.5}$; circumshapes are plotted for $\delta = 0.015$. As in the previous example, the data was translated to the upper right quadrant.

Figure 11 illustrates results for $f(x, y) = x^{1.5} + 10y^{1.5}$; circumshapes are plotted for $\delta = 0.015$. The data was translated to the upper right quadrant. Although the shapes appear constant along one coordinate direction, compression of the circumshapes occurs from row to row.

Figure 12 illustrates results for $f(x, y) = \frac{1}{4} \left(\frac{100}{\sqrt{x^2 + y^2}} - \sqrt{-400 + \frac{10000}{x^2 + y^2}} \right)^2$, a surface derived from perspective projection considerations with $z_{proj} = -100$. The circumshapes shown are derived from the convex hull corresponding to the triangulation; a sampling of circumshapes are shown for clarity. Because this convex body was not defined for all points on the 2D plane, the data set was scaled by a factor of $\frac{2}{3}$ in both coordinate directions. Note that the alternative approach results in circumshapes similar in orientation and eccentricity to the true perspective approach which follows.

Figure 13 illustrates results for perspective projection; $z_{proj} = -100$, $\delta = 0.05$. Because the projection from $z_{proj} = -100$, was not defined for all points, the data set was scaled by a factor of $\frac{2}{3}$ in both coordinate directions. The circumshapes exhibit radial variation in orientation, with eccentricity increasing for increasing distance from the origin.

6   Conclusion

We have demonstrated how a modification of the lifting map formulation which derives a triangulation from the convex hull of a convex body can be used to produce alternatives to the Delaunay triangulation. By suitable construction of the convex body, triangulations can then be "biased" to produce stretched or high aspect ratio triangulations. The appeal of this

method is that a valid triangulation of the point set will always exist for a corresponding convex body, and the method can be generalized to higher dimensions.

References

[1] M.-A. K. Posenau and D. M. Mount. Delaunay triangulation and computational fluid dynamics meshes. In *Proceedings of the Fourth Canadian Conference on Computational Geometry*, pages 316–321, August 1992.

[2] Timothy J. Barth. Numerical aspects of computing viscous high reynolds number flows on unstructured meshes. *AIAA 29th Aerospace Sciences Meeting*, January 1991.

[3] Rainald Lohner and Paresh Parikh. Generation of three-dimensional unstructured grids by the advancing-front method. *AIAA 26th Aerospace Sciences Meeting*, January 1988. AIAA Paper AIAA-88-0515.

[4] J. Peraire, K. Morgan, and J. Peiro. Unstructured finite element mesh generation and adaptive procedures for cfd. *AGARD FDP: Specialist's Meeting*, May 1989.

[5] Dimitri J. Mavriplis. Adaptive mesh generation for viscous flows using delaunay triangulation. *Journal of Computational Physics*, 90(2):271–291, October 1990.

[6] L. P. Chew and R. L. Drysdale. Voronoi diagrams based on convex distance functions. *Proceedings of the 1st Annual ACM Symposium on Computational Geometry*, pages 235–244, 1985.

[7] Herbert Edelsbrunner. *Algorithms in Combinatorial Geometry*. Springer-Verlag, New York, New York, 1987.
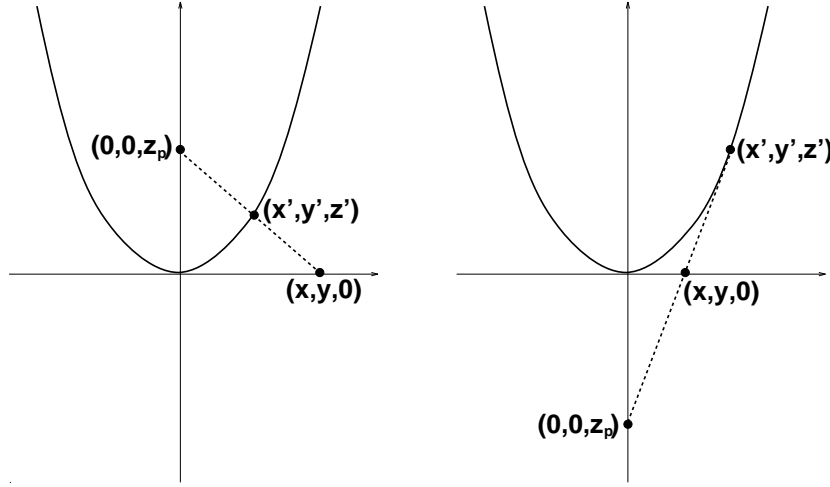
Figure 2: The relationship between points on the plane and on the paraboloid (in cross-section). (a) $z_p > 0$; (b) $z_p < 0$

A   Derivation of Perspective Projection Circumshape Function

Given the equations for a paraboloid, $z' = x'^2 + y'^2$, a plane, $z' = ax' + by' + c$, and a projection point $(0, 0, z_p)$, the circumshapes on the 2D plane can be determined in the following manner. Using similar triangles from the diagrams in Figure 2, the following relationships hold:

Figure 2a:

$$\frac{z_p}{z'} = \frac{x}{x - x'} = \frac{y}{y - y'}$$

Figure 2b:

$$\frac{-z_p + z'}{z'} = \frac{x'}{x' - x} = \frac{y'}{y' - y}$$

Both cases yield:

$$z' = \frac{z_p(x - x')}{x}$$

$$x' = x\left(1 - \frac{z'}{z_p}\right)$$

$$y' = y\left(1 - \frac{z'}{z_p}\right)$$

Substituting the expressions for x' and y' in the plane equation yields:

$$z' = ax\left(1 - \frac{z'}{z_p}\right) + by\left(1 - \frac{z'}{z_p}\right) + c$$

or

$$z' = z_p\frac{ax + by + c}{ax + by + z_p}$$

for $ax + by + z_p \neq 0$. Substituting the expressions for x' and y' in the paraboloid equation yields:

$$z' = x^2(1 - \frac{z'}{z_p})^2 + y^2(1 - \frac{z'}{z_p})^2$$

$$z' = (x^2 + y^2)(1 - \frac{z'}{z_p})^2$$

$$z' = (x^2 + y^2)(1 - 2\frac{z'}{z_p} + \frac{z'^2}{z_p^2})$$

$$z'z_p^2 = (x^2 + y^2)(z'^2 - 2z'z_p + z_p^2)$$

rearranging gives

$$z'^2(x^2 + y^2) - z'(2z_p(x^2 + y^2) + z_p^2) + z_p^2(x^2 + y^2) = 0$$

Substitute the equation for z' from the plane equation into the last result:

$$\left(z_p\frac{ax + by + c}{ax + by + z_p}\right)^2 (x^2 + y^2) - z_p\frac{ax + by + c}{ax + by + z_p}\left((2z_p(x^2 + y^2) + z_p^2) + z_p^2(x^2 + y^2)\right) = 0$$

Expanding and rearranging gives:

$$(x^2 + y^2)(1 - \frac{c}{z_p})^2 - (ax + by + c)(\frac{ax}{z_p} + \frac{by}{z_p} + 1) = 0$$
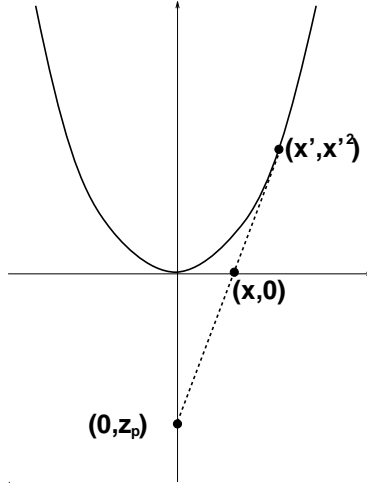
Figure 3: The 2D problem of determining x'.

B Derivation of Body from Perspective Projection

The goal is to derive an expression for a body $f(x, y)$ where orthogonal projection is used with a z value which would have been obtained from perspective projection.

The symmetry of the paraboloid about the z-axis can be exploited to derive an expression which performs as required.

First consider the 2D perspective projection problem shown in Figure 3, where $z_{proj} < 0$. The goal is to find an expression $f(x) = x'$ such that $g(x') = x'^2$, or $g(f(x)) = x'^2$. From consideration of similar triangles:

$$\frac{-z_{proj}}{x} = -\frac{x'^2 - z_{proj}}{x'}$$

Rearranging in terms of x' gives:

$$x'^2 + \frac{z_{proj}}{x}x' - z_{proj} = 0$$

Solving for x' yields $f(x)$:

$$f(x) = x' = \frac{1}{2}\left[\frac{-z_{proj}}{x} \pm \sqrt{\frac{z_{proj}^2}{x^2} + 4z_{proj}}\right]$$

and $g(f(x))$ is

$$g(f(x)) = x'^2 = \frac{1}{4}\left[\frac{-z_{proj}}{x} \pm \sqrt{\frac{z_{proj}^2}{x^2} + 4z_{proj}}\right]^2$$

Because the paraboloid is circularly symmetric about the z-axis, it may be observed that by looking at planes through the z-axis, the 3D problem is identical to the 2D problem.

The goal is to find an expression $h(x, y) = z'$. In the 2D problem, x is the distance from the z-axis. For a 3D formulation, first find the distance to the point under consideration on the 2D plane, which is $\sqrt{x^2 + y^2}$. Then use this new "x'" in the 2D formulation (which is also equivalent to decomposing this value into its x' and y' components and calculating the paraboloid value). This substitution yields

$$z' = \frac{1}{4}\left(-\frac{z_{proj}}{\sqrt{x^2 + y^2}} - \sqrt{4z_{proj} + \frac{z_{proj}^2}{x^2 + y^2}}\right)^2$$

In this case, the negative square root produces the correct behavior for the function, i.e., a convex object.
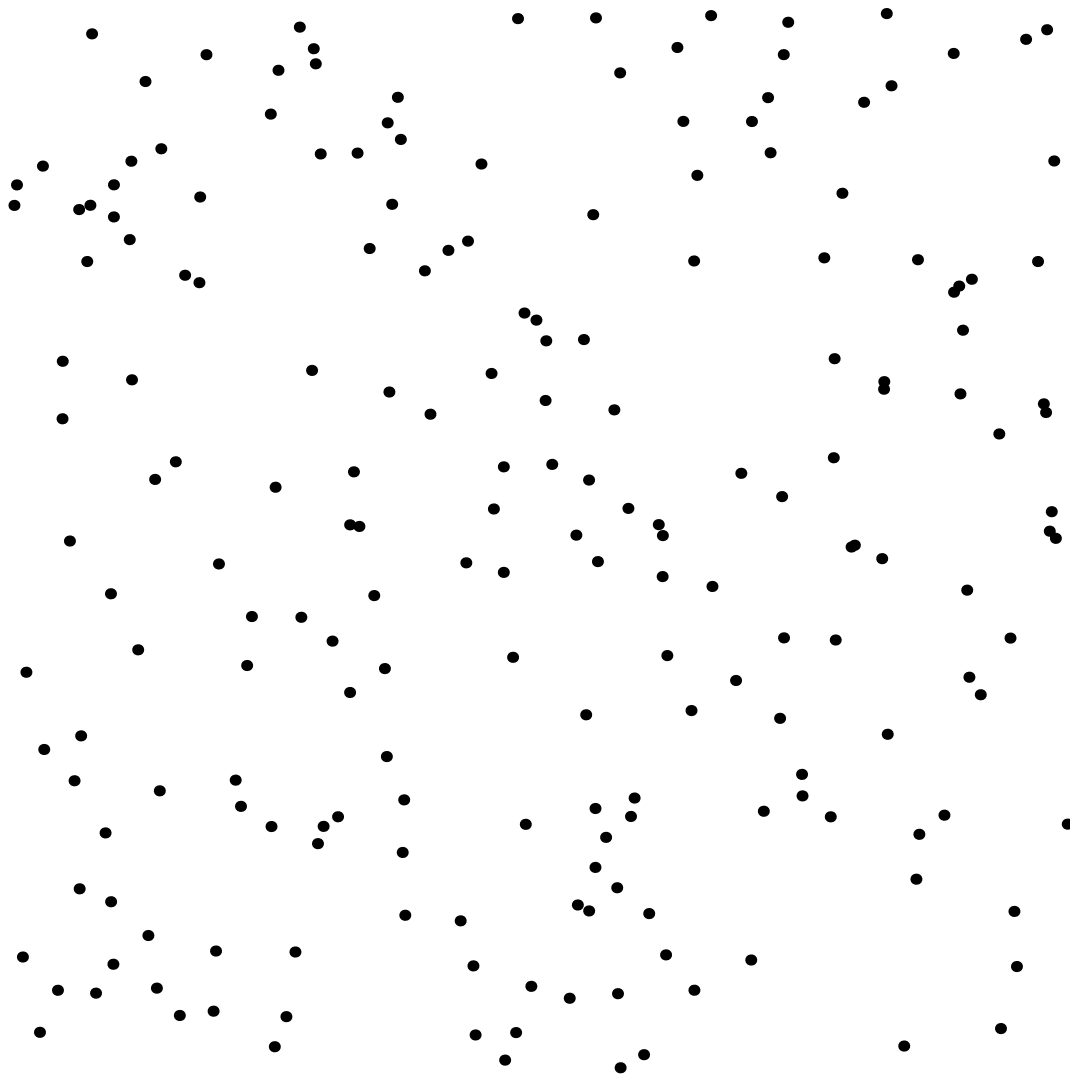
Figure 4: Test data used for all examples.
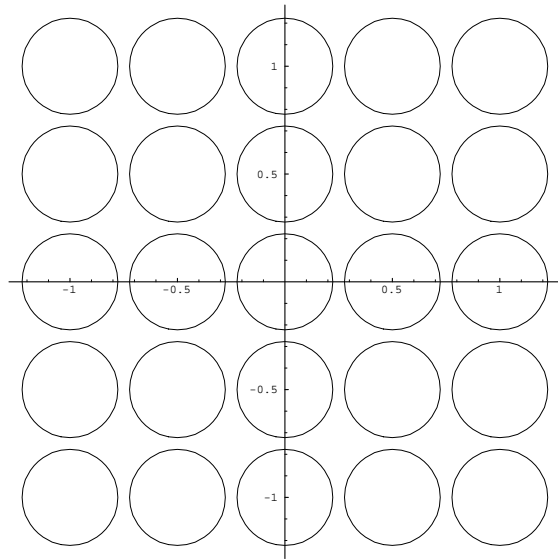
Figure 5a: Circumshapes derived from paraboloid $x^2 + y^2$
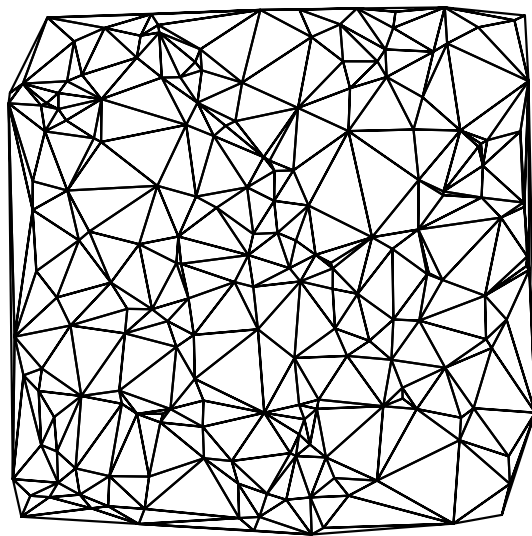
Figure 5b: Triangulation derived from paraboloid $x^2 + y^2$
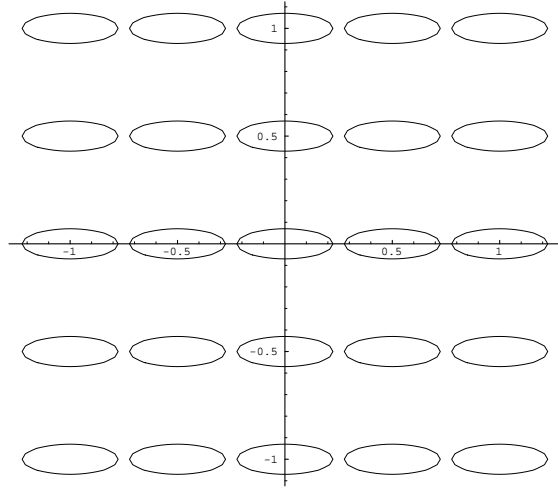
Figure 6a: Circumshapes derived from $x^2 + 10y^2$, $\delta = 0.05$
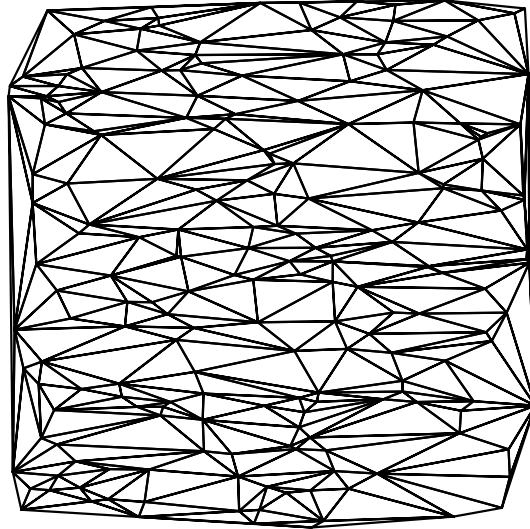
Figure 6b: Triangulation derived from $x^2 + 10y^2$
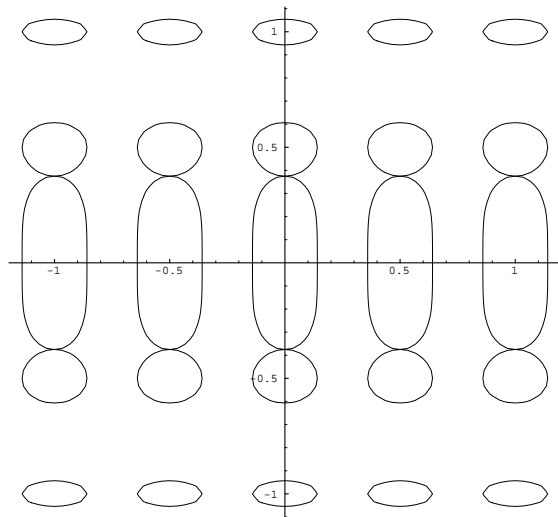
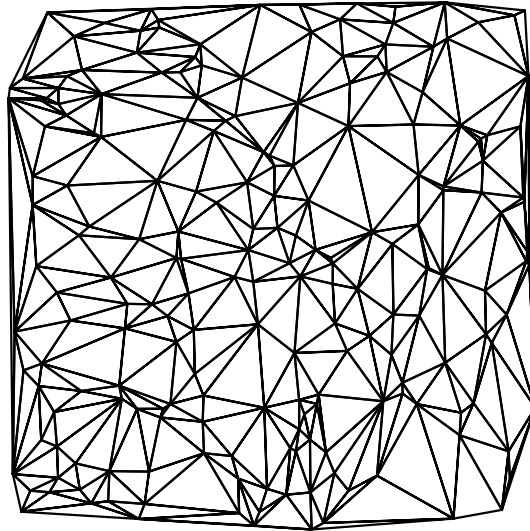Figure 7a: Circumshapes derived from $x^2 + y^4$, $\delta = 0.02$
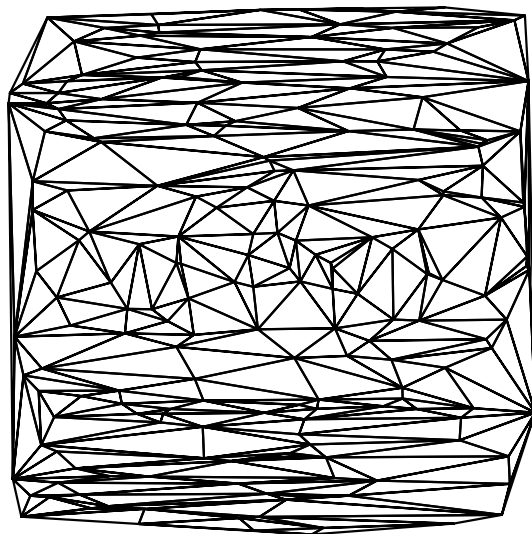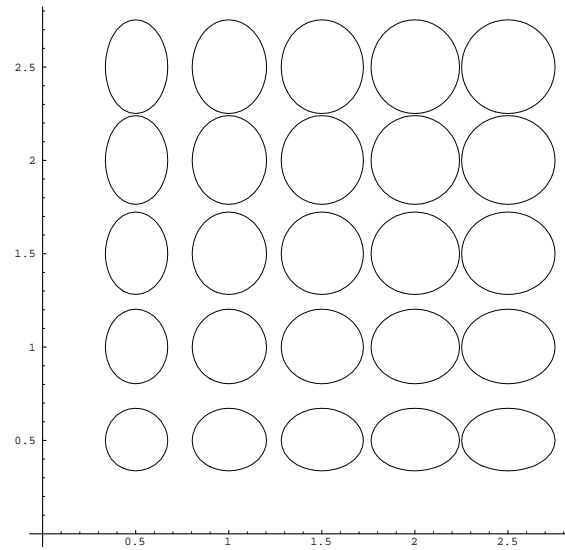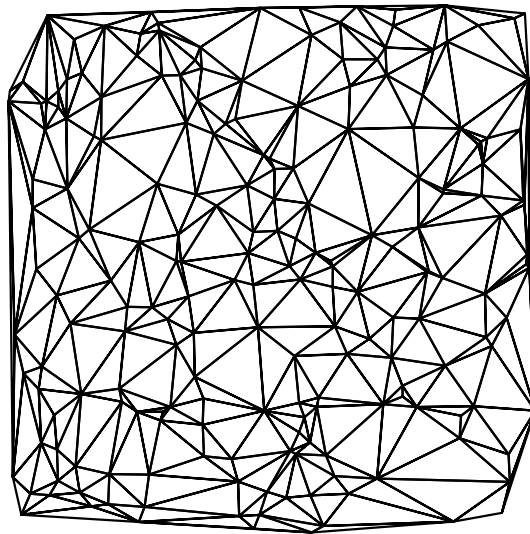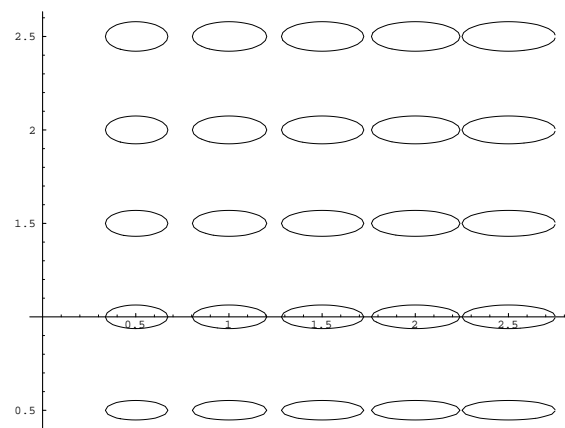

Figure 7b: Triangulation derived from $x^2 + y^4$

14
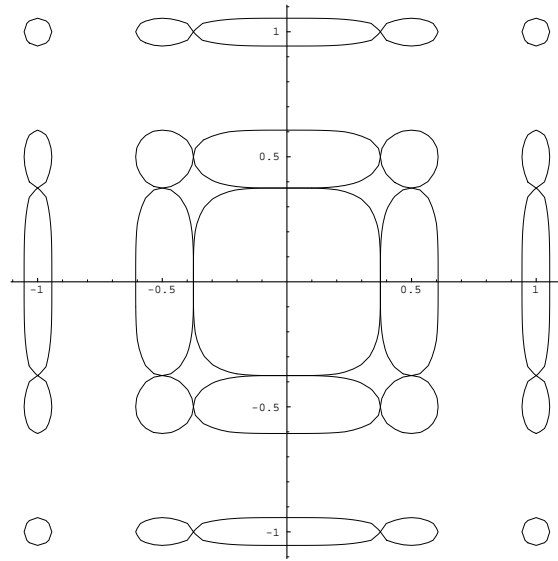
Figure 8a: Circumshapes derived from $x^4 + y^4$, $\delta = 0.02$
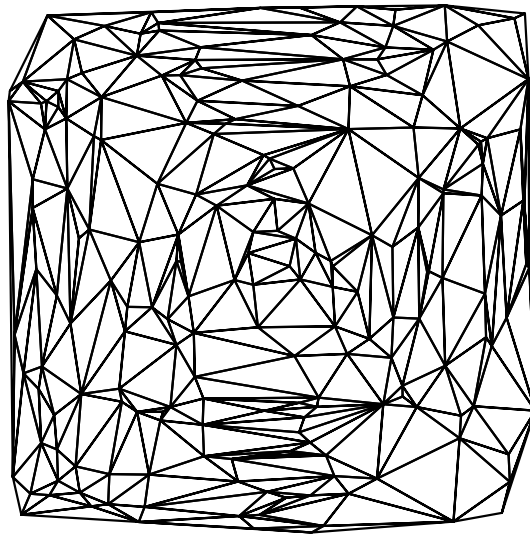
Figure 8b: Triangulation derived from $x^4 + y^4$

15
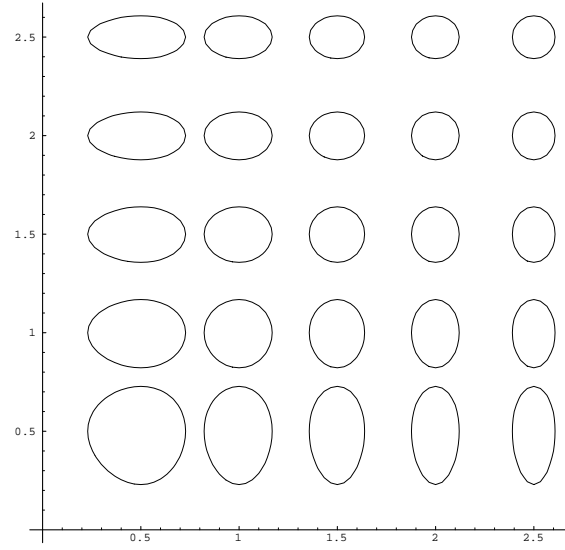
Figure 9a: Circumshapes derived from $x^3 + y^3$, $\delta = 0.09$

Figure 9b: Triangulation derived from $x^3 + y^3$

16

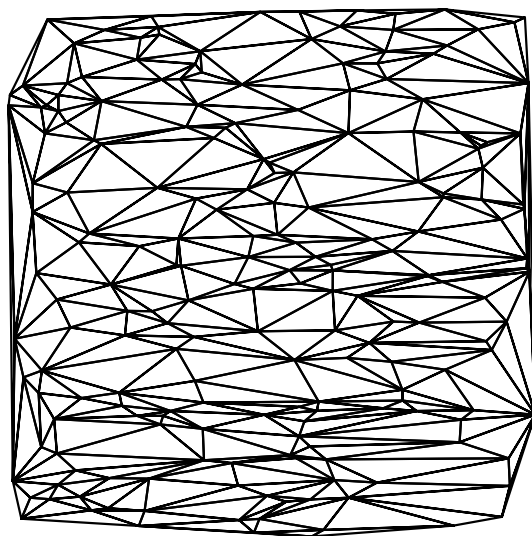Figure 10a: Circumshapes derived from $x^{1.5} + y^{1.5}$, $\delta = 0.015$

Figure 10b: Triangulation derived from $x^{1.5} + y^{1.5}$

17

Figure 11a: Circumshapes derived from $x^{1.5} + 10y^{1.5}$, $\delta = 0.015$

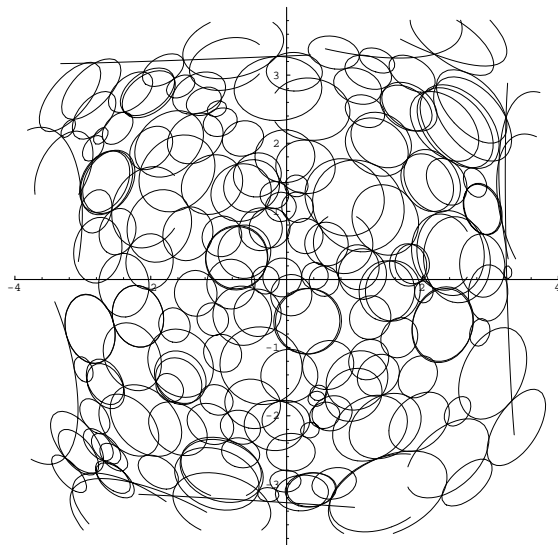
Figure 11b: Triangulation derived from $x^{1.5} + 10y^{1.5}$

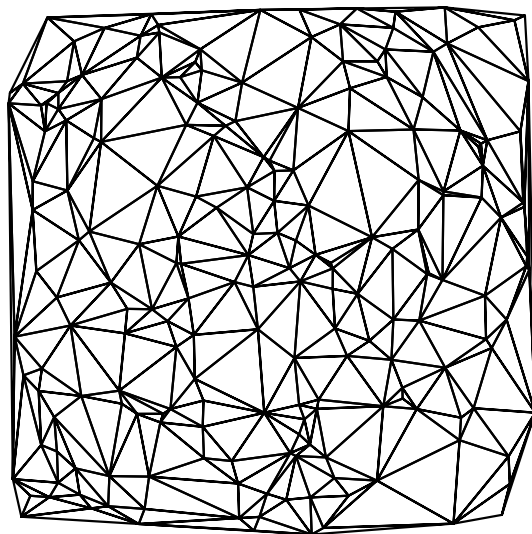Figure 12a: Circumshapes derived from triangulation in Figure 12b

Figure 12b: Triangulation derived from $z = \frac{1}{4} \left(-\frac{z_{proj}}{\sqrt{x^2+y^2}} - \sqrt{4z_{proj} + \frac{z_{proj}^2}{x^2+y^2}} \right)^2$
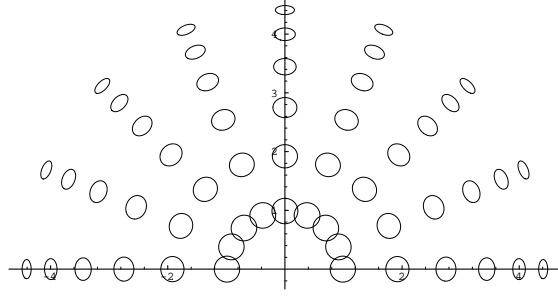
Figure 13a: Circumshapes predicted from perspective projection, $z_{proj} = -100$, $\delta = 0.05$
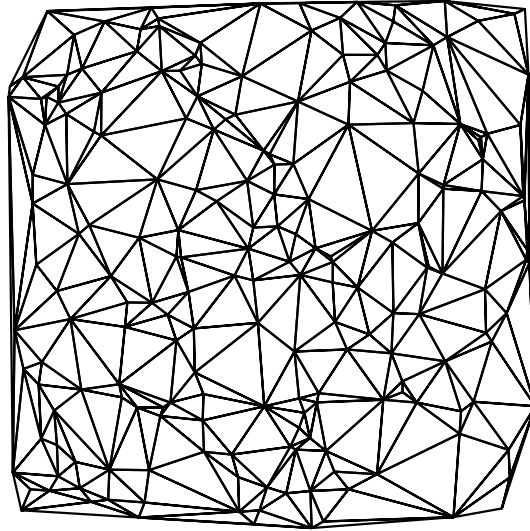

Figure 13b: Triangulation derived from perspective projection, $z_{proj} = -100$